This is the Pre-Published Version.

The following publication Y. Yang, S. Li, H. Yan and W. Jin, "Low-Noise Closed-Loop FOG Driven by Two Broadband Sources," in Journal of Lightwave Technology, vol. 37, no. 18, pp. 4555-4559, 15 Sept., 2019 is available at https://doi.org/10.1109/JLT.2019.2910543.

Low Noise Closed-loop FOG Driven by Two Broadband Sources

Yuanhong Yang*, Shuai Li, Han Yan and Wei Jin

***Abstract*—We propose and demonstrate experimentally a low noise closed-loop fiber optic gyroscope (FOG) driven by two broadband sources simultaneously. The basic characteristic of built-up super broadband light source (SBLS) consists of two superluminescent diodes (SLDs) with different wavelengths was designed and analyzed. The dispersion characteristic of half-wave voltage of multifunction integrated optical circuit (MIOC) was investigated theoretically and experimentally. The tested results agree well with the theoretical model and confirm that the customized MIOC can operate well over a large spectral bandwidth. An experimental FOG driven by the SBLS was built with a solid-core polarization maintaining photonic crystal fiber coil and the closed-loop operation was realized well. Its bias drift and scale factor were tested preliminarily and high performance is achieved compared with the FOGs with single SLD source.**

***Index Terms*—Broadband source, fiber optic gyroscope, multifunction integrated optical circuit, photonic crystal fiber.**

I. Introduction

FIBER optic gyroscope (FOG) with unique characteristics of long life, high reliability, and light weight, has been widely used in various applications and reached good performance in terms of noise (i.e., angle random walk or ARW) and bias drift [1]-[3]. Most of noises in FOG, including coherent backscatters, shot and thermal noises in photoreceiver are largely depressed by use of a high power broadband source, leaving the excess source relative intensity noise (RIN) as the dominate noise contributor [4], [5]. Techniques are developed to reduce the RIN and good performance has been achieved, including the RIN subtraction electronically [6] and optical subtraction [7], adding a high-pass active optical filter or an interferometric filter after the source [8], [9] and letting FOG operate at a bias point close to π instead of π/2 [10], etc. Recently, we investigated theoretically and experimentally the dispersion of half-wave voltage (V_π) of multifunction integrated optical circuit (MIOC) and confirmed the customized MIOC can work with a very large broadband range [11]. In this paper, we expand this work and demonstrate experimentally a low noise closed-loop FOG driven by two broadband sources simultaneously. An equivalent super-broadband light source (SBLS) was built up and tested with two superluminescent diodes (SLDs) with different wavelengths simultaneously. Because the RIN is simply the inverse of the spectrum width and this can be regarded as another effective way to depress RIN and ultra-low noise may be achieved by combining existing techniques for the FOG driven by the proposed SBLS. The dispersion characteristic of V_π of MIOC was then investigated theoretically and experimentally. The tested results agree well with the theoretical model and confirm that the customized MIOC can operate well over a super broadband range. Whereafter, an experimental FOG driven by the SBLS was built and the fiber coil was wound with ~1km solid-core polarization maintaining photonic crystal fiber (PM-PCF) coil. The closed-loop operation was realized well with the customized MIOC and the SBLS. Their bias drifts and scale factors were tested preliminarily, the noise of FOG was depressed greatly compared with the FOGs with single SLD source and the scale factor nonlinear error is not degraded.

This work was supported by National Natural Science Foundation of China under Grant U1637106, 61227902 and National Key R&D Program of China 2018YFC1503703 and Program for Innovative Research Team in University under Grant IRT 1203.

Y. H. Yang, S. Li and H. Yan are with the Department of Measuring and Control and Information Technology, School of Instrumentation and Optoelectronic Engineering, Beihang University, 100191, Beijing, China (e-mail: yhyang@buaa.edu.cn, lishuai1994@buaa.edu.cn, yanhan_17@buaa.edu.cn).

W. Jin is with the Department of Electrical Engineering, The Hong Kong Polytechnic University, Hong Kong, China (email: eewjin@polyu.edu.hk).

II. Structure and Operation Principle

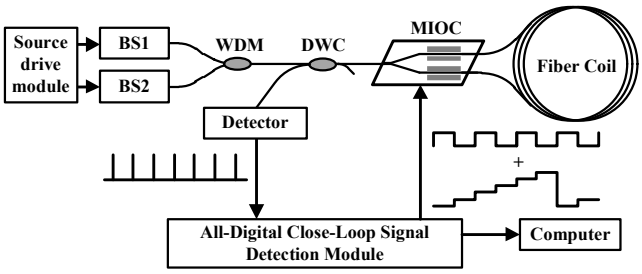

Fig. 1. Schematic of FOG driven by two broadband sources.

The schematic of closed-loop FOG driven by two broadband sources is shown in Fig. 1. Lights from two broadband sources (BS1 and BS2) with respective mean wavelengths of λ1 and λ2 are combined by use of a wavelength division multiplexer (WDM) to act as one equivalent SBLS of FOG. The dual window coupler (DWC) which can operate at two wavelengths simultaneously is taken to lead the lights from two sources into Sagnac interferometer assembly (SIA) and lead the backward interference light from SIA to detector. The SIA is composed of a custom-made MIOC and a fiber coil. The MIOC is fabricated specially and can operate at λ1 and λ2 with balanced insert loss

©2019 IEEE. Personal use of this material is permitted. Permission from IEEE must be obtained for all other uses, in any current or future media, including reprinting/republishing this material for advertising or promotional purposes, creating new collective works, for resale or redistribution to servers or lists, or reuse of any copyrighted component of this work in other works.

and the cut-off wavelength of fibers used in optical circuit is all short enough and the condition of the single-mode propagation can be guaranteed at λ1 and λ2 simultaneously. An all-digital closed-loop signal detection module and a computer are used for signal processing and record.

In FOG, the angle random walk (ARW) is a measure of random phase noise, such as thermal noise, photo shot noise in the detector, electronic and relative intensity noises. All the main noise factors under the auxiliary modulation depth π/2 can be evaluated according to the following equation [12]:

$$ARW = \frac{\sqrt{2}\lambda c}{2\pi LD}\sqrt{\frac{4kT}{R\eta^2P^2}+\frac{ei_d}{\eta^2P^2}+\frac{e}{\eta P}+\frac{\lambda^2}{4c\Delta\lambda}} \quad (1)$$

where λ is the operational wavelength, c is light velocity in vacuum, L and D are the fiber length and diameter of fiber coil respectively, k is Boltzmann's constant, T is absolute temperature, R is resistance of the trans-impedance transduce of the photo-detector device, η is efficiency ratio of photodiode, P is incident light power on photodiode, e is elementary charge, i_d is photodiode dark-current, $\Delta\lambda$ is spectral width of source. The forth term in the square root function is the well-known RIN and will become a dominant noise and other noises can be depressed to acceptable level when P is big enough. The RIN is simply the inverse of the spectrum width and this indicates that increasing the bandwidth of source is the effective method to reduce RIN.

The mean wavelength $\bar{\lambda}$ and bandwidth $\Delta\lambda$ of the SBLS proposed can be computed by using the following equations [13]:

$$\bar{\lambda} = \frac{\sum P(\lambda_i)\lambda_i}{\sum P(\lambda_i)} \quad (2)$$

$$\Delta\lambda = \frac{\left[\sum P(\lambda_i)\Delta\lambda_i\right]^2}{\sum P^2(\lambda_i)\Delta\lambda_i} \quad (3)$$

where, $P(\lambda_i)$ and λ_i are the power and wavelength corresponding to sampling point i, $\Delta\lambda_i$ is the sampling interval. The SBLS may have a very broadband equivalent bandwidth if the distance between the two broadband sources and their bandwidths are large enough. For example, when we take two SLDs with wavelengths of 1310nm and 1550nm and bandwidths of 51nm and 49nm as BS1 and BS2 respectively, the computed equivalent wavelength and spectral bandwidth will be 1430nm and 152nm respectively, that is much greater than any of them. And the ARW may be decreased ~2 times approximatively. In addition, the spectrum of each source can be adjusted independently and the high stability of mean-wavelength of the SBLS may be obtained with a special current and temperature control circuit. This implies low noise and high stability scale factor may be achieved simultaneously.

III. Super-Broadband Source Design and Analysis

As mentioned above, two SLDs were taken as the SBLS of FOG and a special source driver circuit was designed for the two SLDs. As shown in Fig. 2, The diode chip temperature of each SLD is controlled independently with automatic temperature control circuit (ATC) by using of the integrated thermoelectric cooler (TEC) and negative temperature resistance (NTR) in the module, while the diode chips in series are driven by same current with an automatic current control circuit (ACC). This design can guarantee that the two SLDs operate with one accord. The built-up SBLS outputs from the common port of WDM and the typical spectrum is shown in Fig. 3. The combined spectrum of the SBLS is fitted here as a Gaussian function and the main parameters of the SLDs and the SBLS are listed in Table IV and the SBLS bandwidth is 151.99nm, far wider than that of single SLD.

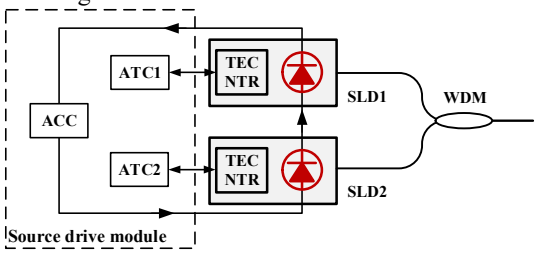

Fig. 2. Schematic of SBLS built with two SLDs.

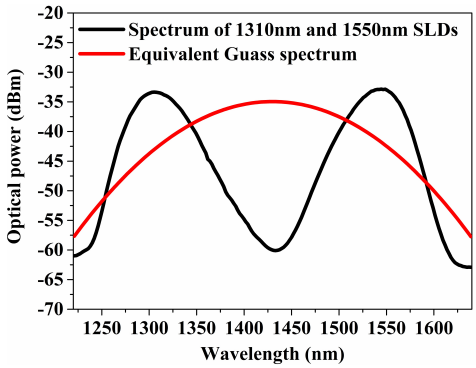

Fig. 3. Typical spectrum of SLDs and the built-up SBLS.

Fig. 4 shows the output optical power of SLDs measured simultaneously with a two channel powermeter (Agilent 8163A) within ~5 hours under laboratory environment. The curves show their behavior is consistent as we expect.

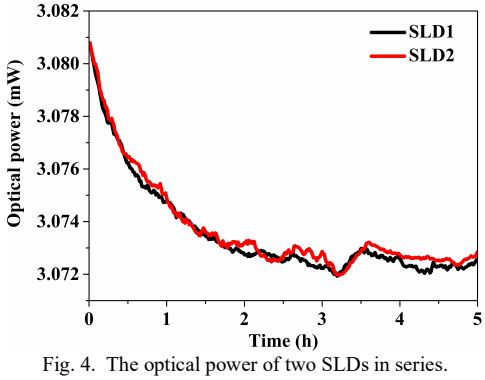

Fig. 4. The optical power of two SLDs in series.

IV. Investigation on V_π Dispersion of MIOC

MIOC is the key component which has a flat response over a large bandwidth and ensures the use of efficient signal-processing techniques for high performance FOG. It is composed of a Y-junction, push-pull phase modulators and high polarization rejection circuit with proton exchange [14]. As shown in Fig. 5, the common model of V_π can be expressed as [15]:

$$V_\pi = \frac{\lambda G}{n_e^3(\lambda)\gamma_{33}(\lambda)\Gamma(\lambda)L} \tag{4}$$

where G is the electrodes spacing, L is the electrode length, n_e is the effective refractive index, γ_{33} is electro-optic coefficient, Γ is overlap integral factor.

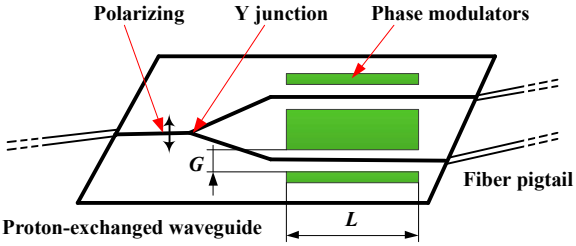

Fig. 5. Schematic of the MIOC.

The model parameters n_e, γ_{33} and Γ are wavelength dependence and can be described by the following equations and the intrinsic coefficients of the typical $LiNbO_3$ crystal are taken from references [16]-[18] and listed in Table I-III.

$$n_e = \left(1 + \frac{A_n\lambda^2}{\lambda^2 - B_n} + \frac{C_n\lambda^2}{\lambda^2 - D_n} + \frac{E_n\lambda^2}{\lambda^2 - F_n}\right)^{1/2} \tag{5}$$

$$\gamma_{33} = A_\gamma + \frac{B_\gamma}{\lambda^2 - C_\gamma} + \frac{D_\gamma}{\lambda^2 - E_\gamma} \tag{6}$$

$$\Gamma = A_\Gamma\lambda^2 + B_\Gamma\lambda + C_\Gamma \tag{7}$$

TABLE I
THE MODEL COEFFICIENTS OF n_e

A_n (a.u.)	B_n (μm^2)	C_n (a.u.)	D_n (μm^2)	E_n (a.u.)	F_n (μm^2)
2.9804	0.02047	0.5981	0.0666	8.9543	416.08

TABLE II
THE MODEL COEFFICIENTS OF γ_{33}

A_γ (pm/V)	B_γ (pm·μm^2/V)	C_γ (μm^2)	D_γ (pm·μm^2/V)	E_γ (μm^2)
27.04426	7.50588	-3.90008	0.75161	0.05138

TABLE III
THE MODEL COEFFICIENTS OF Γ

A_Γ (μm^{-2})	B_Γ (μm^{-1})	C_Γ (a.u.)
-0.17927	0.46521	0.29942

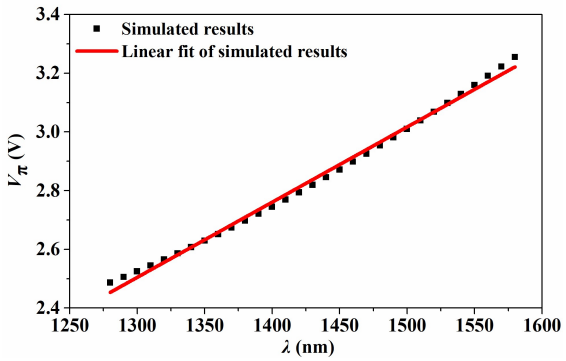

Fig. 6. Simulated curve of V_π vs. λ.

A MIOC was custom designed with G=6μm and L=18mm, and the value of V_π was simulated within wavelength range of 1280nm-1580nm. The simulated curve is monotonous and shown in Fig. 6. The simulated dispersion coefficient of the fitted linear model was obtained as following equation:

$$V_\pi(\lambda) = 0.00256\lambda - 0.82452 \tag{8}$$

where the units of λ and V_π are nm and V respectively.

The V_π was measured too with a precise automatic measurement system based on four steps modulated Sagnac interferometer with 1310nm and 1550nm broadband sources respectively [19]. As shown in Fig. 7, the measurement system is composed of broadband source (BS), tunable filter (TF), dual window coupler, MIOC under tested, fiber coil, detector, digital signal processing module and computer. Because of the perfect reciprocity of Sagnac optical circuit and periodic modulation, the optical circuit loss, possible Sagnac phase shift and ambient temperature fluctuation in this system have no effect on the measurement result and high precision can be achieved.

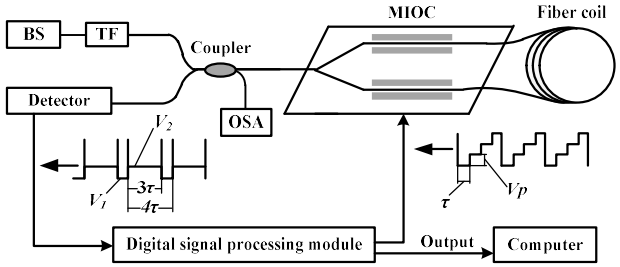

Fig. 7. Schematic of the V_π measurement system, V_p: step height, V_1: output during reset state, V_2: output during other states, τ: propagation time through the sensing loop.

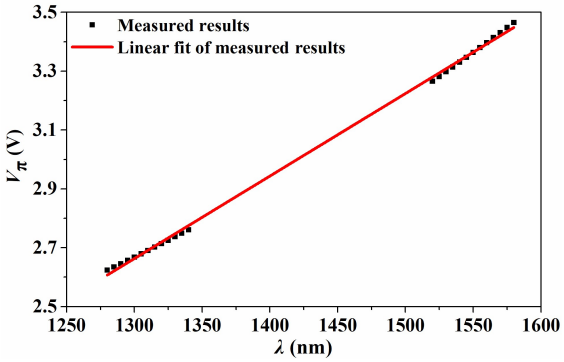

Fig. 8. Measured curve of V_π vs. λ.

Where, the tunable source is built up with the BS and TF (WLTF-1310-60/0.8 and WLTF-1550-60/0.8) and its bandwidth is larger than 0.8 nm to get the trade-off between the signal noise and the wavelength resolution. The tuning range is about 60nm in both 1310nm band (1280nm - 1340nm) and 1550nm band (1520nm - 1580nm). An optical spectrum analyzer (OSA) is used to monitor the filtered source wavelength. The MIOC is custom fabricated and the nominal V_π is 3.37V at 1550nm wavelength under 25°C. The V_π was measured with about 5nm wavelength interval. The sampling interval is 1s and test period is about 30 minutes at each wavelength. The average of V_π and corresponding wavelength were recorded. The tested result is shown in Fig. 8 and a good linear relation between V_π and λ is obtained

within 1310nm and 1550nm bands. The fitted linear curve is gotten and the measured dispersion coefficient is about 2.81×10^{-3} V/nm. The measured results agree well with the simulated theoretical dispersion model and confirm that the MIOC can operate well over a large bandwidth.

V. Experimental Investigation

An experimental FOG was built based on Fig. 1 and a PM-PCF coil was used to guarantee perfectly the condition of the single-mode propagation at λ1 and λ2 because of its characteristic of endless single mode. The main components and their parameters are listed in Table IV. The power of each SLD is bigger than 3mW. And the incident power on detector are 34.22μW, 34.23μW, and 68.45μW for FOG driven by SLD1, SLD2, and SBLS respectively. The RIN will dominate clearly compared to other noises [20].

TABLE IV
The Main Components and Their Parameters

Components	Main parameters
SLD1	λ1=1308.580nm, Δλ1=51.026nm, Power>3mW
SLD2	λ2=1543.271nm, Δλ2=48.870nm, Power>3mW
SBLS	λ=1429.865nm, Δλ=151.99nm
CWDM	1310/1550 CWDM, IL<0.5dB, PDL<0.03dB
DWC	1310±40nm, 1550±40nm, IL<0.5dB, PDL<0.03dB
Detector	InGaAs PIN-FET, 1100nm to 1650nm
Fiber Coil	PM-PCF, ~1km, Diameter: 170mm

CWDM: Coarse Wavelength Division Multiplexing, IL: Insertion Loss, PDL: Polarization Dependent Loss, PM-PCF: Polarization Maintaining Photonic Crystal Fiber

The exact V_π of MIOC operating with SLD1, SLD2 and SBLS were measured respectively with the method described in section IV and closed-loop operation was realized well with each single SLD and the SBLS. Fig. 9 shows the typical modulation waveform (a) with modulation depth π/2 added on MIOC and the output waveform (b) from detector when the FOG was driven by SBLS and the loop was closed. This demonstrates a perfect closed-loop operation state.

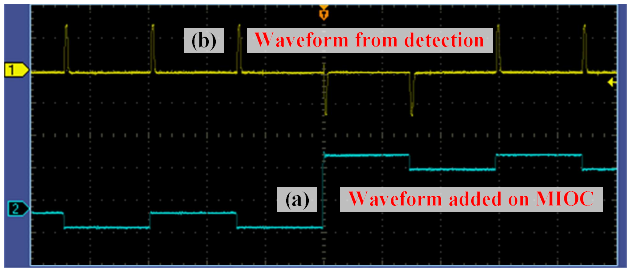

Fig. 9. Closed-loop operation waveform with SBLS.

In the experimental FOG system, SLD1 and SLD2 can work separately or simultaneously by switches control and the performance of FOG driven by SLD1, SLD2, and SLD1&SLD2 (i.e. SBLS) respectively was tested preliminarily under laboratory environment. The tested curves of scale factor, zero bias and Allan variance are shown in Fig. 10, Fig. 11, and Fig. 12 respectively. The scale factor nonlinear errors are 1.716 ppm, 1.669 ppm, and 1.682 ppm within ±150 deg/hr range, the bias drifts (1σ, 100s) are 2.261×10^{-3} °/h, 2.329×10^{-3} °/h, and 8.848×10^{-4} °/h, the ARW values are 4.2×10^{-4} °/$h^{1/2}$, 4.6×10^{-4} °/$h^{1/2}$, and 1.7×10^{-4} °/$h^{1/2}$. These results indicate that the scale factor nonlinear error is not degraded with the built-up SBLS, whereas the bias drift and ARW are reduced obviously. And according to Eq. (1), the ARW value of FOG driven by SBLS is estimated of ~1.9×10^{-4} °/$h^{1/2}$ based on typical parameters listed in Table IV and agrees with the experimental results.

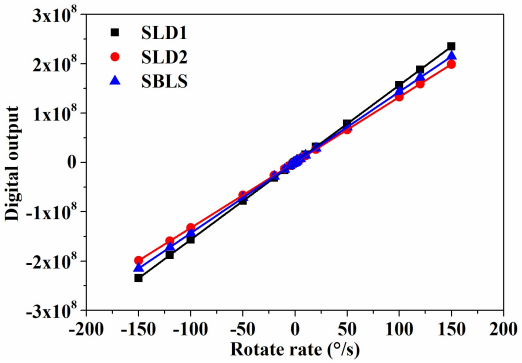

Fig. 10. Scale factor of FOG driven by different sources.

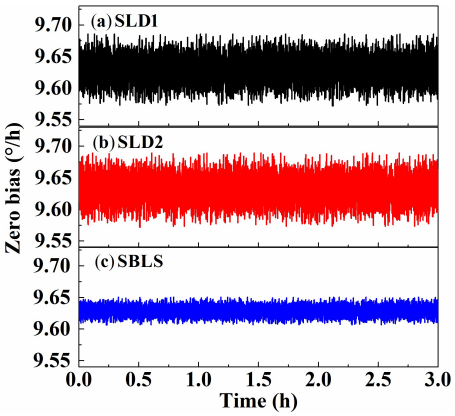

Fig. 11. Zero bias of FOG driven by different sources (1s sampling).

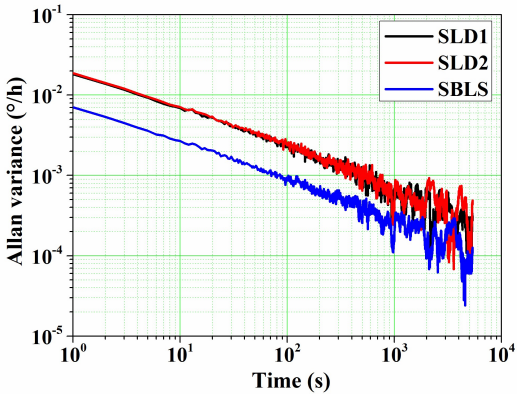

Fig. 12. Allan variance of FOG driven by different sources.

VI. Conclusion

In conclusion, a low noise closed-loop FOG with PM-PCF

coil driven by two broadband sources was proposed and experimentally demonstrated. The basic characteristic of SBLS consists of two SLDs was investigated experimentally. The dispersion model of MIOC was established and V_π of a customized fabricated MIOC was tested precisely. The experimental results confirm that the MIOC can operate well over a large wavelength range of 1310nm and 1550nm bands. An experimental FOG with PM-PCF coil driven by two SLDs with wavelengths of 1310nm and 1550nm was built and tested. The noise of FOG is depressed greatly and the bias drift is reduced effectively. The scale factor nonlinear error is not degraded. The closed-loop FOG driven by two broadband sources may be a promising scheme to realize ultra-precision.

REFERENCES

[1] H. C. Lefèvre, "Potpourri of comments about the fiber optic gyro for its 40th anniversary, and how fascinating it was and it still is!" *Proc. SPIE*, vol. 9852, pp. 985203-1-985203-10, 2016.

[2] G. A. Sanders, *et al*, "Fiber optic gyro development at Honeywell," *Proc. SPIE*, vol. 9852, pp. 985207-1-985207-14, 2016.

[3] Y. Paturel, J. Honthaas, H. Lefèvre, and F. Napolitano, "One nautical mile per month FOG-based strapdown inertial navigation system: A dream already within reach?" *Gyroscopy and Navigation*, vol. 5, no. 1, pp. 1-8, 2014.

[4] J. N. Blake, G. A. Sanders, and L. K. Strandjord, "Fiber optic gyroscope output noise reducer," U.S. Patent 5 469 257, Nov. 21, 1995.

[5] K. Iwatsuki, "Excess noise reduction in fiber gyroscope using broader spectrum linewidth Er-doped superfluorescent fiber laser," *IEEE Photonic Technol. Lett.*, vol. 3, no. 3, pp. 281-283, Mar. 1991.

[6] R. P. Moeller and W. K. Burns, "1.06 μm all-fiber gyroscope with noise subtraction," in *8th Optical Fiber Sensors Conference*, Monterey, CA, USA, 1992, pp. 82-85.

[7] R. P. Moeller and W. K. Burns, "Low noise fiber gyroscope system which includes excess noise subtraction," U.S. Patent 5 331 404, Jul. 19, 1994.

[8] F. Hakimi and J. D. Moores, "RIN-reduced light source for ultra-low noise interferometric fibre optic gyroscopes," *Electronic Lett*., vol. 49, no. 3, pp. 205-206, Jan. 2013.

[9] J. Honthaas, J. Bonnefois, E. Ducloux, and H. Lefèvre, "Interferometric filtering of the excess relative intensity noise of the broadband source of a fiber optic gyroscope," *Proc. SPIE*, vol. 9157, pp. 91572D-1-91572D-4, 2014.

[10] H. C. Lefèvre, S. Vatoux, M. Papuchon, and C. Puech, "Integrated optics: A practical solution for the fiber-optic gyroscope," *Proc. SPIE*, vol. 719, pp. 101-112, 1986.

[11] Y. Yang, F. Yang, and H. Yan, "Investigation on dispersion of V_π of multifunction integrated optical circuit," in *26th International Conference on Optical Fiber Sensors*, 2018, paper ThE74.

[12] Yu. N. Korkishko, *et al*, "Highest bias stability fiber-optic gyroscope SRS-5000," in *Inertial Sensors and Systems*, 2017, paper P03.

[13] Y. Yang, *et al*, "Erbium-doped superfluorescent fiber source for fiber optic gyroscope," *Proc. SPIE*, vol. 4920, pp. 111-114, 2002.

[14] P. G. Suchoski, T. K. Findakly, and F. J. Leonberger, "$LiNbO_3$ integrated optical components for fiber optic gyroscopes," *Proc. SPIE*, vol. 993, pp. 240-244, 1988.

[15] S. Chen, J. Cheng, and W. Gao, "A phase modulation method for improving the scale factor stability of Fiber-Optic Gyroscope," in *IEEE International Conference on Mechatronics & Automation*, Takamatsu, Japan, 2009, pp. 37-42.

[16] D. E. Zelmon, D. L. Small, and D. Jundt, "Infrared corrected Sellmeier coefficients for congruently grown lithium niobate and 5 mol.% magnesium oxide-doped lithium niobite," *J. Opt. Soc. Am. B*, vol. 14, no. 12, pp. 3319-3322, Dec. 1997.

[17] K. Yonekura, L. Jin, and K. Takizawa, "Measurement of dispersion of effective electro-optic coefficients r_E^{13} and r_E^{33} of non-doped congruent $LiNbO_3$ crystal," *Jpn. J. Appl. Phys.*, vol. 47, no. 7, pp. 5503-5508, Jul. 2008.

[18] J. Li, D. Lu, and Z. Qi, "Analyses of wavelength dependence of the electro-optic overlap integral factor for $LiNbO_3$ channel waveguides," *Acta Phys. Sin.*, vol. 63, no. 7, pp. 077801-1-077801-7, 2014.

[19] Y. Yang and H. Yu, "Digital measuring scheme for half-wave voltage of Y-tap multiple integrated optical circuit," *Chinese Opt. Lett.*, vol. 2, no. 11, pp. 640-642, Nov. 2004.

[20] F. Guattari, S. Chouvin, C. Moluçon, and H. Lefèvre, "A simple optical technique to compensate for excess RIN in a fiber-optic gyroscope," in *Inertial Sensors and Systems*, 2014, paper P10.